Crystal Structure of F65A/Y131C-Methylimidazole Carbonic Anhydrase V Reveals Architectural Features of an Engineered Proton Shuttle†

Kevin M. Jude,‡ S. Kirk Wright,§,|| Chingkuang Tu,⊥ David N. Silverman,⊥ Ronald E. Viola,§ and David W. Christianson*,‡

Roy and Diana Vagelos Laboratories, Department of Chemistry, University of Pennsylvania, Philadelphia, Pennsylvania 19104-6323, Department of Pharmacology, University of Florida College of Medicine, Gainesville, Florida 32610-0267, and Department of Chemistry, University of Toledo, Toledo, Ohio 43606

Received September 26, 2001; Revised Manuscript Received December 12, 2001

ABSTRACT: The crystal structure of F65A/Y131C murine α-carbonic anhydrase V (CAV), covalently modified at cysteine residues with 4-chloromethylimidazole, is reported at 1.88 Å resolution. This modification introduces a methylimidazole (MI) group at residue C131 in the active site with important consequences. F65A/Y131C-MI CAV exhibits an up to 3-fold enhancement of catalytic activity over that of wild-type CAV [Earnhardt, J. N., Wright, S. K., Qian, M., Tu, C., Laipis, P. J., Viola, R. E., and Silverman, D. N. (1999) *Arch. Biochem. Biophys. 361*, 264−270]. In this modified CAV variant, C131-MI acts as a proton shuttle, facilitating the deprotonation of a zinc-bound water molecule to regenerate the nucleophilic zinc-bound hydroxide ion. A network of three hydrogen-bonded water molecules, across which proton transfer likely proceeds, bridges the zinc-bound water molecule and the C131-MI imidazole group. The structure of F65A/Y131C-MI CAV is compared to structures of Y64H/F65A murine CAV, wild-type human α-carbonic anhydrase II, and the γ-carbonic anhydrase from *Methanosarcina thermophila* in an effort to outline common features of catalytic proton shuttles.

The carbonic anhydrases (CAs)[1] comprise a family of zinc metalloenzymes that catalyze the reversible hydration of carbon dioxide, $CO_2 + H_2O \leftrightarrow HCO_3^- + H^+$ (*1*−*3*). There are 10 known active α-CA isozymes in mammals: CA I−VII, IX, XII, and XIV (*4*). The best-studied isozyme is CAII from the erythrocyte, which operates near the limit of diffusion control with a k_{cat}/K_M of 1.5×10^8 M^{-1} s^{-1} (*5*). In blood, the biological function of this isozyme is to facilitate bicarbonate transfer from the erythrocyte to the pulmonary capillary. Another interesting isozyme is mitochondrial CAV. Primarily found in liver, CAV maintains bicarbonate production for ureagenesis and gluconeogenesis (*6*). CAV is a slightly less efficient enzyme with a maximal k_{cat}/K_M of 3×10^7 M^{-1} s^{-1} (*7*). The crystal structures of both isozymes provide important reference points for interpreting kinetic data. The human CAII structure was first reported by Liljas and colleagues (*8*) and more recently refined at 1.54 Å resolution (*9*), and the murine CAV structure has been determined at 2.45 Å resolution (*10*). Related by a level of amino acid sequence identity of 53%, human CAII and murine CAV have similar backbone conformations.

Kinetics experiments with both CAII and CAV indicate a similar sequential reaction for CO_2 hydration, in which the interconversion of CO_2 and HCO_3^- (eq 1) precedes the regeneration of the zinc-bound hydroxide ion via a series of proton transfer steps [eq 2 (*7*)]:

$$CO_2 + EZn^{2+}OH^- \rightleftharpoons EZn^{2+}HCO_3^-(+H_2O) \rightleftharpoons EZn^{2+}H_2O + HCO_3^- \quad (1)$$

$$X{-}EZn^{2+}H_2O + B \rightleftharpoons XH^+{-}EZn^{2+}OH^- + B \rightleftharpoons X{-}EZn^{2+}OH^- + BH^+ \quad (2)$$

In eq 2, X is a protein residue that serves as a proton shuttle, accepting a proton from zinc-bound solvent and then transferring the proton to buffer B in solution. In both CAII and Y64H/F65A CAV, H64 is implicated as the proton shuttle residue; moreover, the intramolecular proton transfer between ZnH_2O and X in eq 2 is the rate-limiting step of k_{cat} for CO_2 hydration (*11*−*13*). In CAII, this proton transfer is more properly described as a proton translocation, i.e., a series of proton transfer reactions between hydrogen-bonded water molecules (*1*, *9*). Proton translocation along such a "proton wire" is described as Grotthuss diffusion (*14*, *15*), whereby a series of proton hopping steps across the wire is followed by reorientation of the water molecules, priming the wire for the next proton transfer.

† This work was supported by NIH Grants GM45614 (D.W.C.) and GM25154 (D.N.S.) and NSF Grant MCB0196103 (R.E.V.).

* To whom correspondence should be addressed. Telephone: (215) 898-5714. Fax: (215) 573-2201. E-mail: chris@xtal.chem.upenn.edu.
‡ University of Pennsylvania.
§ University of Toledo.
|| Current address: Department of Biochemistry, University of Wisconsin, Madison, WI 53706.
⊥ University of Florida College of Medicine.

[1] Abbreviations: CA, carbonic anhydrase; CAII, human carbonic anhydrase II; CAV, murine carbonic anhydrase V; Cam, *M. thermophila* carbonic anhydrase; Zn−Cam, Cam with a Zn^{2+} ion in the active site; Co−Cam, Cam with a Co^{2+} ion in the active site; 4-CMI, 4-(chloromethyl)imidazole; C131-MI, Cys131 modified with 4-CMI to yield Cys131-methylimidazole; PEG, polyethylene glycol; MES, 2-(*N*-morpholino)ethanesulfonic acid; NCS, noncrystallographic symmetry; rms, root-mean-square.

10.1021/bi015808q CCC: $22.00
Published on Web 01/31/2002

In contrast, wild-type CAV is as much as 20-fold less active than CAII due in part to the presence of Y64, which does not play a significant role in catalysis (*7*, *13*). Mutagenesis studies suggest that multiple residues may act as proton shuttles in CAV, with alanine substitutions of Y131 and K91 having the most deleterious effects on k_{cat} (*16*). However, even the double variant Y131A/K91A CAV retains considerable catalytic activity.

To engineer potential new proton shuttle sites in CAV, Earnhardt and colleagues (*17*) report the modification of site-specific cysteine variants of CAV with the imidazole functional groups 4-(bromoethyl)imidazole and 4-(chloromethyl)imidazole (4-CMI). In variants containing the Y131C substitution, specifically, Y131C and F65A/Y131C CAVs, modification with 4-CMI results in 3-fold faster proton-transfer rates with a pK_a value of 5.8 indicated for the proton shuttle group [for reference, the phenolic hydroxyl group of Y131 is 9.1 Å from zinc-bound solvent (*10*)]. These observations are consistent with the successful introduction of a proton shuttle group resulting from covalent modification of the γ-sulfur atom of C131 with methylimidazole (C131-MI). Although proton transfer rate enhancements measured for C131-MI CAV derivatives do not exceed the 10-fold enhancement previously observed for Y64H/F65A CAV, it is notable that the C131-MI side chain is an efficient proton shuttle, whereas the chemically similar H131 side chain in Y131H CAV is not (*13*). These observations, along with recently published structural and mechanistic studies of proton shuttle trajectories in the γ-CA from *Methanosarcina thermophila*, raise the following thought-provoking question: what structural features in a protein constitute a catalytically efficient proton transfer site?

We now report the 1.88 Å resolution crystal structure of F65A/Y131C-MI CAV to address this question. The crystal structure shows that the imidazole side chain of C131-MI is oriented toward the active site zinc ion and is ~8 Å away from the zinc-bound hydroxide ion. Three intervening water molecules form a hydrogen-bonded "proton wire" that can potentially support proton transfer between the zinc-bound water and N1 of the C131-MI imidazole group. Comparisons of this structure with the structures of Y64H/F65A murine CAV, wild-type human CAII, and the γ-CA from *M. thermophila* allow us to hypothesize about what structural features are important for catalytic proton shuttles.

MATERIALS AND METHODS

The F65A/Y131C variant of an N-terminally truncated form of murine CAV lacking the first 51 residues was overexpressed in *Escherichia coli* and purified as described previously (*7*, *17*). Modification of the enzyme with 4-CMI was performed as described previously (*17*), and the enzyme was confirmed to be >95% modified at four solvent-exposed cysteines. Following modification, the protein buffer was changed to 50 mM Tris-sulfate (pH 8.5) using Microcon-10 concentrators (Amicon).

The modified protein was crystallized by the vapor diffusion method with slight modifications to the conditions employed by Boriack-Sjodin and colleagues (*10*) for the crystallization of the wild-type protein. A hanging drop containing 3 μL of a protein solution (6 mg/mL), 0.5 μL of 1.2 mM sucrose monolaurate, and 3 μL of precipitant buffer [12% PEG 8000, 100 mM MES (pH 6.7), 100 mM sodium acetate, and 1 mM dithiothreitol] was suspended over a 1 mL reservoir of precipitant buffer. With a pK_a of 5.8 (*17*), C131-MI is predominantly (90%) uncharged at pH 6.7. Diamond-shaped, platelike crystals appeared within 3 days and formed prisms within 3−4 weeks. Prior to data collection, crystals were quickly transferred through a series of drops in which 2, 4, and 6 μL, successively, of PEG 400 had been diluted to 20 μL with precipitant buffer. Crystals were then flash-cooled in liquid nitrogen. X-ray diffraction data to 1.88 Å resolution were collected at the Brookhaven National Laboratory, beamline X12B, at the National Synchrotron Light Source (Upton, NY) using an ADSC Quantum-4 CCD detector. Data were integrated and reduced using the HKL suite of programs (*18*). Diffraction data were indexed in space group *C*2 with the following unit cell parameters: $a = 99.3$ Å, $b = 66.7$ Å, $c = 92.6$ Å, $\alpha = \gamma = 90°$, and $\beta = 105.7°$, with two molecules in the asymmetric unit. Data reduction statistics are recorded in Table 1.

Table 1: Data Collection and Refinement Statistics for F65A/Y131C-MI CAV

no. of crystals	1
no. of measured reflections	141410
no. of unique reflections	46312
maximum resolution (Å)	1.88
completeness of data (outer shell)	96.8% (87.9%)
R_{merge}[a]	0.051 (21.7)
no. of water molecules in the final cycle of refinement	471
total no. of atoms in the final cycle of refinement	4334
no. of reflections used in refinement (25.0−1.88 Å)	44468
R_{work}[b]	0.191
R_{free}[c]	0.222
rms deviation from ideality	
bonds (Å)	0.006
angles (deg)	1.3
dihedral angles (deg)	25
improper dihedral angles (deg)	0.8

[a] R_{merge} for replicate reflections; $R = \sum|I_h - \langle I_h\rangle|/I_h$, where I_h is the intensity measured for reflection h and $\langle I_h\rangle$ is the average intensity for reflection h calculated from replicate data. [b] Crystallographic R factor; $R_{work} = \sum||F_o| - |F_c||/\sum|F_o|$, where $|F_o|$ and $|F_c|$ are the observed and calculated structure factor amplitudes, respectively, for those reflections not included in the R_{free} test set. [c] Free R factor; $R_{free} = \sum||F_o| - |F_c||/\sum|F_o|$ for only those reflections included in the R_{free} test set.

Initial phases were obtained by molecular replacement using the program amore (*19*, *20*). The atomic coordinates of wild-type CAV refined at 2.45 Å resolution (*10*) were obtained from the RCSB Protein Data Bank (*21*). Prior to use as a probe for rotation and translation searches, the protein model was modified to remove water molecules and to remove molecule B of the protein as well as to truncate residues 65 and 131 to alanine. Using intensity data in the 25.0−2.55 Å resolution shell in a cross-rotation search yielded two solutions with peak heights of 33.2σ ($\alpha = 116.43°$, $\beta = 63.76°$, and $\gamma = 81.50°$ and $\alpha = 63.57°$, $\beta = 116.24°$, and $\gamma = 261.50°$), corresponding to two molecules in the asymmetric unit. Subsequent translation searches yielded solutions with peak heights of 39.1σ and 45.3σ ($T_x = 0.1731$, $T_y = 0.0000$, and $T_z = 0.4079$ and $T_x = 0.8281$, $T_y = 0.0158$, and $T_z = 0.919$, respectively). Rigid-body refinement of the two molecules using all intensity data in the 25.0−1.88 Å resolution shell reduced the crystallographic

R factor (R_{work}) from 0.53 to 0.42. Placement of the two molecules in the asymmetric unit was performed using the program lsqkab (*19*). The graphics program O was used for visualizing the protein model and for fitting electron density maps (*22*).

Crystallographic refinement was performed using the program CNS (*23*). Initial refinement employed torsional molecular dynamics with energy minimization, using the maximum likelihood algorithm, as well as grouped *B* factor refinement. Strict noncrystallographic symmetry (NCS) constraints were employed in the early stages of refinement. The Sγ atom of C131 corresponded to a strong peak in the $|F_o| - |F_c|$ map. Following two rounds of grouped *B* factor refinement, *B* factor refinement of individual atoms lowered R_{work} from 0.306 to 0.279 and R_{free} from 0.325 to 0.296. NCS constraints were converted to restraints to facilitate identification of methylimidazole prosthetic groups that might adopt different conformations in the two molecules of the asymmetric unit. Appropriate weights for these restraints were guided by the behavior of R_{free}. Assignment of 132 water molecules further lowered R_{work} to 0.242 and R_{free} to 0.261. Water placement was performed using the automatic water picking function of CNS, and waters were accepted or rejected by visual inspection of difference electron density maps. Specifically, water molecules were built into electron density peaks of $>3\sigma$ that were within hydrogen bonding distance of at least one polar protein atom or two other water molecules hydrogen bonded to polar protein atoms; the minimization of R_{free} in refinement indicated that these newly built water molecules were introduced reliably.

Electron density peaks corresponding to non-protein zinc ligands were interpreted as acetate and water, which was similar to the interpretation described in the crystal structure of carbonic anhydrase XII (*24*). Following the initial interpretation of well-ordered water molecules associated with the protein model, electron density for a methylimidazole prosthetic group attached to C188 of molecule A was unambiguous. Coordinates for the modified residue were constructed using the program macromodel (*25*), and topology and refinement parameters were calculated with the program xplo2d (*26*−*28*). Following addition of more water molecules, the methylimidazole prosthetic groups of C188, molecule B, and C131, molecule A, were added to the model. Interpretation of electron density maps indicated two conformations for the C131-MI side chain. The methylimidazole prosthetic group of C131, molecule B, was disordered and accordingly modeled as an unmodified cysteine. Electron density for a Cδ atom was identified next to C183 of molecules A and B, but no imidazole group was visible in the electron density. Therefore, C183 in both molecules was modeled as *S*-methylcysteine. Grouped occupancy refinement was performed on methylimidazole prosthetic groups, acetates, and a K^+ ion in the final model. Final refinement statistics are presented in Table 1. Atomic coordinates have been deposited in the RCSB as entry 1KEQ.

RESULTS AND DISCUSSION

Structure of F65A/Y131C-MI CAV. No major structural changes occur as a consequence of the F65A/Y131C substitutions or of the covalent modification with 4-CMI, and there are no local changes at the other sites of modification in the protein. A Cα alignment of molecules A and B in the asymmetric unit yields a root-mean-square (rms) deviation of 0.32 Å, while a similar alignment of molecule A of the present structure with that of wild-type CAV yields an rms deviation of 0.35 Å. Three residues at the N-terminus (S22−E24) and seven residues at the C-terminus (D263−S269) are not visible in electron density maps and are therefore excluded from the final model. However, L262, which was excluded from the final model of wild-type CAV, is clearly visible in $2|F_o| - |F_c|$ and $|F_o| - |F_c|$ omit maps of F65A/Y131C-MI CAV and is therefore included in the final model.

The F65A/Y131C variant of CAV contains five cysteine residues, four of which are solvent accessible: C74, C183, C188, and the engineered C131. Studies utilizing Ellman's reagent and the papain amplification assay (*29*) indicate a single free cysteine residue in this variant modified with 4-CMI, consistent with a stoichiometry of four modified cysteine residues (*17*). The side chains of C74, C183, and C188 are on the "backside" of the enzyme, away from the lip of the active site cleft, so they are too far from the active site to participate directly in catalysis (*10*, *17*). Only C131 is in the enzyme active site, so only modification of this residue should impact proton transfer steps in catalysis.

The flexible nature of a cysteine−methylimidazole side chain, which contains four torsional degrees of freedom, apparently renders crystallographic visualization difficult due to conformational mobility. Out of eight modified side chains in the asymmetric unit of the crystal, only three complete prosthetic groups are interpretable and modeled: those at C188 of molecules A and B and that at C131 of molecule A. Since the C131-MI side chain is the residue of interest, this structure provides the necessary data for interpreting previous kinetic measurements (*17*).

The electron density corresponding to the imidazole group of C131-MI in molecule A is rather broad and is interpreted to reflect two slightly different conformations, related by 10°, 10°, and 170° rotations about side chain torsion angles χ_2, χ_3, and χ_4, respectively. In conformer 1, the imidazole group contacts the amide group of Q92 and a water molecule (O577). In conformer 2, the imidazole makes an additional contact with a second water molecule (O475). A network of three hydrogen-bonded water molecules (O707− O480− O577) bridges zinc-bound solvent and N1 of the C131-MI side chain (Figure 1a). These water molecules have thermal *B* factors between 28 and 36 Å^2 (overall average water *B* factor = 26 Å^2). Hydrogen bond distances in this network are in the range of 2.6−3.1 Å, and hydrogen bond geometries are generally good. However, O577 forms a slightly distorted hydrogen bond (Figure 2). This distortion, combined with the relatively high *B* factor of water 577 (36 Å^2) and with the two conformations of the C131-MI side chain, suggests that some solvent reorganization and C131-MI conformational changes must occur to support efficient proton transfer to C131-MI.

In molecule B, the C131-MI side chain is disordered, presumably due to excessive conformational mobility (Figure 1b). Additionally, the hydrogen-bonded solvent network appears to be incomplete, with only water 687 (which corresponds to water 480 in molecule A) observed in the final model.

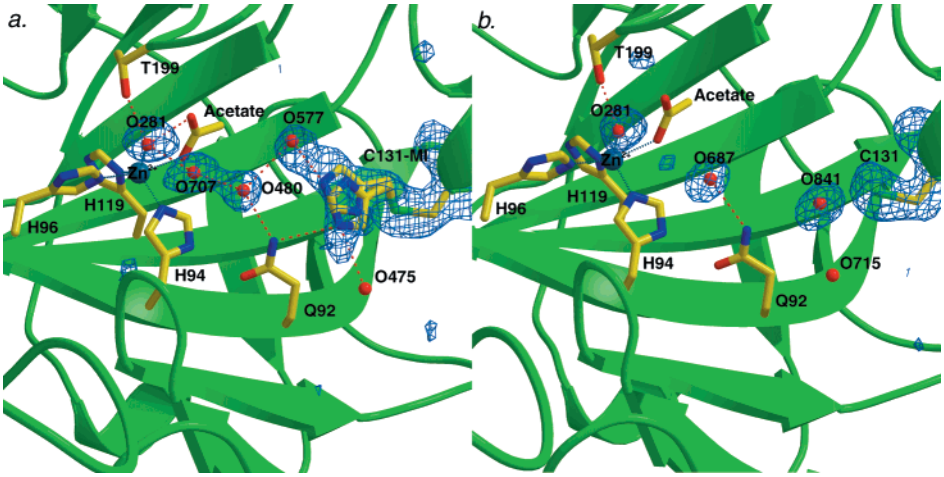

FIGURE 1: Difference electron density map calculated with Fourier coefficients $|F_o| - |F_c|$ (contoured at 3.5σ) of F65A/Y131C-MI CAV molecules A (a) and B (b). Residue 131, zinc-bound hydroxide, and water molecules 480, 577, 687, 707, and 841 were omitted from the final model prior to the structure factor calculation. The methylimidazole group in molecule A is interpreted to adopt two conformations; that of molecule B lacks well-defined electron density and is interpreted to be conformationally disordered.

Molecules A and B each contain five-coordinate zinc ions. Protein ligands to Zn^{2+} are H94, H96, and H119; non-protein ligands are acetate anion and a solvent molecule. Acetate is an analogue of the product bicarbonate, and the binding mode of acetate in this structure is similar to that observed in acetate complexes with carbonic anhydrases II (*9*, *30*) and XII (*24*). The binding mode of acetate mimics a five-coordinate complex that presumably occurs in catalysis, in which the addition of a water molecule to a tetrahedral zinc−bicarbonate complex yields an intermediate five-coordinate complex. Subsequent bicarbonate departure returns the zinc coordination polyhedron to a tetrahedral zinc−solvent complex and facilitates ionization to yield zinc-bound hydroxide. Thus, although the structure of F65A/Y131C-MI CAV is that of an inhibited enzyme, the inhibitor is a product analogue and the enzyme−inhibitor complex mimics the state of the enzyme immediately preceding the proton transfer step mediated by Y131C-MI.

Structural Aspects of Proton Shuttles in the Carbonic Anhydrases. CAV is effectively transformed into an analogue of CAII, the prototypical carbonic anhydrase isozyme, by the double mutation Y64H/F65A. However, the crystal structure of this double variant is not sufficiently well determined, at 2.8 Å resolution, to discern a hydrogen-bonded water bridge between zinc-bound hydroxide and H64 (*13*). Therefore, comparison of the 1.88 Å resolution F65A/Y131C-MI CAV structure to the 1.54 Å resolution human CAII structure [PDB entry 2CBA (*9*)] is more instructive. A Cα alignment of molecule A of F65A/Y131C-MI CAV with CAII yields an rms deviation of 1.1 Å. The active site clefts of the two enzymes are shown in Figure 3. Both enzymes contain a network of hydrogen-bound water molecules that bridge zinc-bound solvent and the proton shuttle group, and some of these water molecules make hydrogen bond interactions with other active site residues. However, there are two major differences between the water bridges of the two enzymes. First, the water bridges adopt different trajectories, toward opposite sides of the active site cleft. Second, the water bridge in F65A/Y131C-MI CAV contains three water molecules, and that of CAII contains two water molecules.

It is reasonable to expect that catalytic proton transfer occurs over the experimentally observed water bridges in CAII and F65A/Y131C-MI CAV. Although additional, highly exchangeable water molecules are certainly present in the enzyme active site, they are transparent to crystallographic analysis. Participation of such water molecules in catalytic proton transfer would require a lengthening of the proton wire. However, the complete translocation of a rate-limiting bonding defect in a proton wire is considerably slower for longer chains of water molecules (i.e., more than two to four) due to barriers to solvent reorientation (*31*). Therefore, the most efficient proton wire will be simply the shortest possible proton wire, i.e., as observed in the crystal structures of these enzymes.

Differences in the trajectories of catalytic proton translocation between CAII and F65A/Y131C-MI CAV help explain structure−activity relationships in other CAV variants. In Y64H/F65A CAV, the smaller side chain at position 65 is required for catalysis due to the restriction of H64 mobility and to the perturbation of the water bridge to H64 by the bulky F65 side chain (*13*). In contrast, F65A/Y131C-MI CAV is catalytically identical to Y131C-MI CAV, demonstrating that the F65 side chain does not hinder the effectiveness of C131-MI as a proton shuttle. A phenyl group at position 65 would not perturb the proton transfer trajectory across the water bridge in F65A/Y131C-MI CAV (Figure 3).

In view of enhanced proton transfer rates in F65A/Y131C-MI CAV (*17*), it is perhaps surprising that proton transfer rates are not enhanced in C131H CAV (*13*). Although each variant contains a newly introduced imidazole group at position 131, the naturally occurring histidine imidazole group of C131H CAV is on a shorter side chain than that of F65A/Y131C-MI CAV. Thus, an additional water molecule would have to join the hydrogen-bonded water network between zinc-bound solvent and the C131H imidazole to complete a proton wire. The lack of enhanced proton transfer in this variant suggests that a satisfactory proton wire cannot be formed. As noted previously, the complete translocation of a bonding defect in a proton wire is considerably slower for longer chains of water molecules (i.e., more than two to

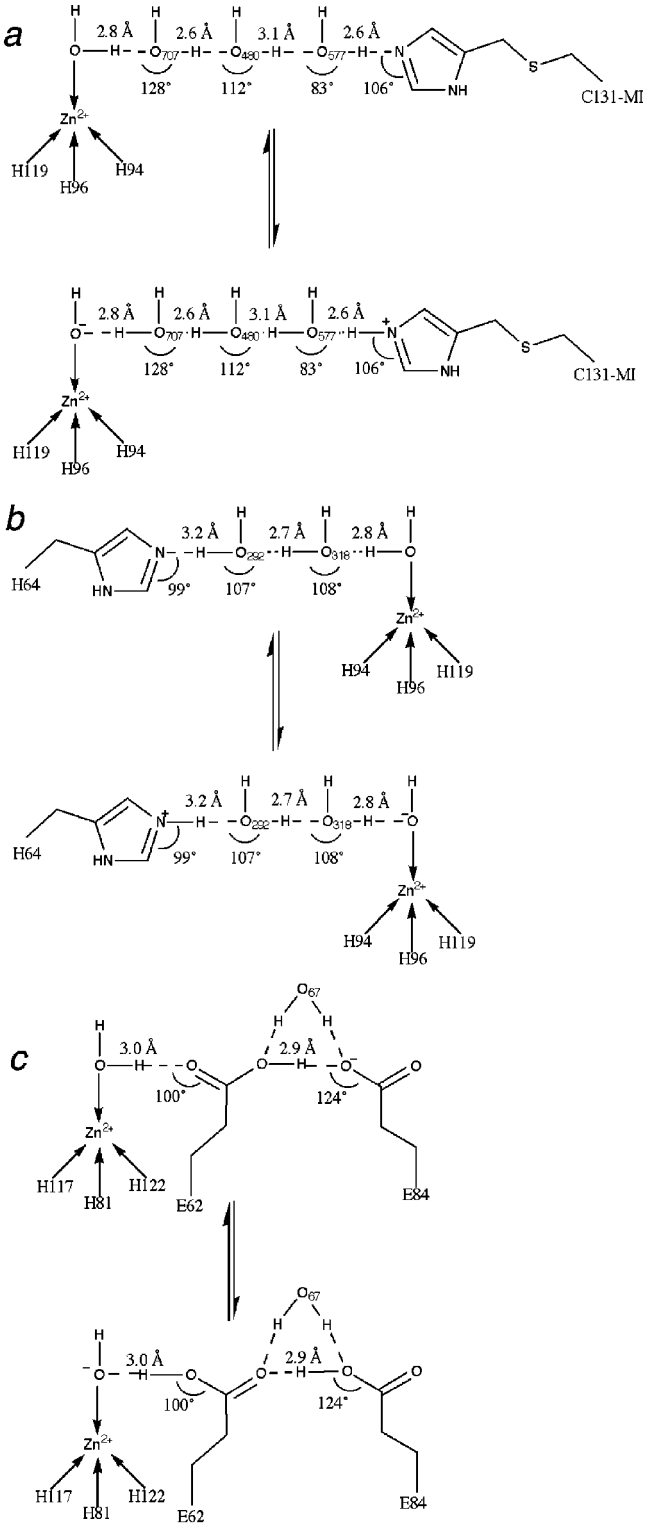

FIGURE 2: Schematic diagrams of proton wires that support intramolecular proton transfer. Hydrogen bond lengths and angles are shown and indicate geometries of hydrogen donor and acceptor atoms: (a) F65A/Y131C-MI murine CAV (this work), (b) wild-type human CAII (*9*), and (c) γ-CA from *M. thermophila* (*34*).

four) due to reorientation barriers (*31*). Perhaps the catalytic advantage of a H131 proton shuttle is compromised by the increased number of water molecules required to link zinc-bound solvent and H131.

It is puzzling that the electron density maps of Figure 1 reveal that C131-MI in molecule A adopts two partially occupied conformations, whereas C131-MI in molecule B appears to be completely disordered. Biochemical studies indicate complete covalent modification of all solvent-exposed cysteine residues (*17*). At the very least, these results indicate that C131-MI is capable of some degree of conformational mobility. Notably, H64 of CAII adopts two conformations related by a 64° rotation about torsion angle χ_1 (*9*, *32*). Thus, conformational mobility appears to be a hallmark of histidine or imidazole proton shuttles in catalysis, and as noted above, C131-MI has two additional torsion angles about which rotations can occur. That catalysis by H64A CAII is rescued by the addition of exogenous imidazole demonstrates that even an "infinitely mobile" imidazole supports proton transfer (*11*), so long as the catalytic imidazole functionality can adopt a fixed and appropriately oriented position long enough to accept the proton product.

Is conformational mobility a hallmark of other functional groups that serve as catalytic proton shuttles? In the γ-carbonic anhydrase of *M. thermophila* (Cam), the carboxylate group of E84 functions as the proton shuttle, with a pK_a of 6.9 (*33*). Iverson and colleagues (*34*) observed three distinct conformations of E84 in a collection of crystal structures of Cam complexed with Zn^{2+}, Co^{2+}, bicarbonate ion, and sulfate ion. In the structure of Cam complexed with Zn^{2+} (Zn−Cam), two conformations of E84 are observed. In conformer 1, E84 is hydrogen bonded to E62, which is hydrogen bonded to zinc-bound solvent; in conformer 2, E84 is oriented away from the active site. A third conformation of E84, which is also oriented away from the active site, is present in other structures (Figure 4).

In the Zn−Cam structure, the carboxylate group of E62 would appear to substitute for the water molecules of a two-water proton wire. Tripp and Ferry (*33*) suggest that the proximity of E62 and E88 is responsible for the elevated pK_a of the principal proton shuttle residue, E84. This hypothesis is confirmed by the presence of a hydrogen bond between the side chains of E62 and E84, indicating that the two residues share a proton at pH 7.0. Two possible routes of proton transfer are suggested by the Zn−Cam structure (Figure 4); E62 abstracts a proton from zinc-bound solvent and then transfers a proton directly either to E84 or to E84 via a water molecule, O67 (*34*). However, kinetic studies of E62 variants of Cam do not confirm the role of E62 as a proton shuttle residue and suggest that a proton wire composed entirely of water molecules may exist between zinc-bound solvent and E84 (*33*).

In conclusion, we hypothesize that simple architectural features may characterize effective proton shuttle sites in the CAs. First, a hydrogen-bonded solvent bridge between the proton donor and the proton shuttle group is required. Given that a hydrogen bond defines the reaction coordinate of proton transfer, the presence of hydrogen-bonded water networks bridging zinc-bound solvent and the proton shuttle in the structures of CAII (*9*) and F65A/Y131C-MI CAV suggests that proton transfer occurs via the Grotthuss mechanism, rather than via hydrodynamic diffusion. In the Grotthuss mechanism, the propagation of an ionic defect ("proton hopping" step) is followed by the rate-limiting propagation of a bonding defect ("reorientation" or "turn" step) in which the network is restored (*14*, *15*, *31*). Theoretical studies of the 23 Å long ion channel gramicidin A suggest

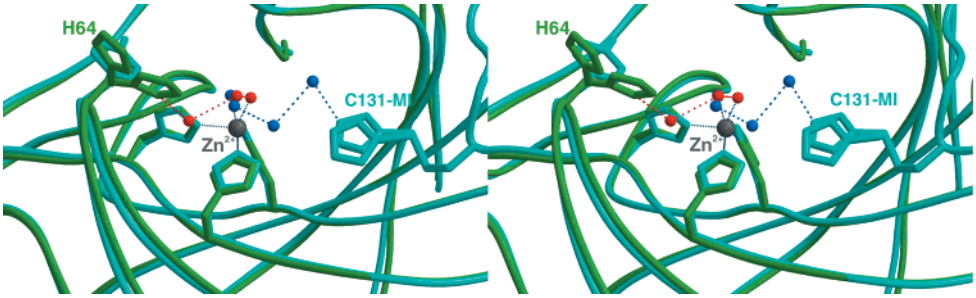

FIGURE 3: Stereoview of a Cα alignment (rms deviation of 1.1 Å) of CAII (green) and F65A/Y131C-MI CAV (blue), illustrating the divergent trajectories of the proton wires bridging zinc-bound solvent and the proton shuttle group in each enzyme.

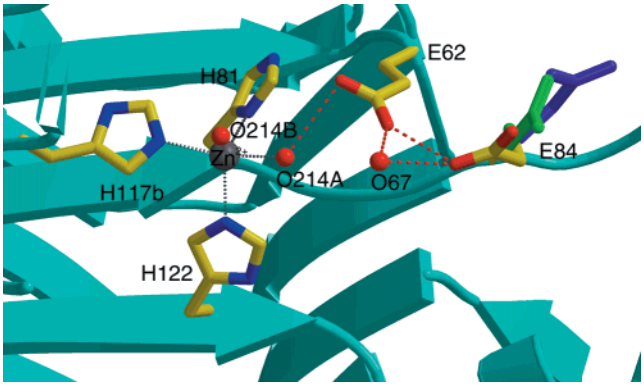

FIGURE 4: Active site of γ-CA from *M. thermophila*, complexed with Zn^{2+}. Conformer 2 of E84 is shown in green, while conformer 3, from the structure of γ-CA complexed with Co^{2+} and bicarbonate, is shown in purple. Hydrogen bond interactions are represented by red dashed lines (*34*).

that the proton transfer rate is maximal in the highly polarized region near the excess charge, while fluctuations distant from the positive charge hinder proton hopping over long distances (*31*). The donor−acceptor distance of 7−8 Å observed for CA proton shuttles may limit the effect that structural fluctuations can exert on the proton transfer rate.

In the absence of a periodic channel structure, as seen in gramicidin A, the length of an effective proton wire is limited by the occurrence of bonding defects within the wire. In the carbonic anhydrases discussed here, the experimentally observed number of water molecules in a proton wire appears to be two to three. Possibly, longer proton wires in rapid biological catalysis are limited by increasing activation barriers for solvent reorientation; theoretical studies by Pomès indicate that "the complete translocation of a bonding defect is a considerably slower process in chains of more than 2 to 4 water molecules" (*31*). In Cam, these waters are apparently replaced with an acidic amino acid side chain that increases the pK_a of the principal proton shuttle residue, E84, to 6.9 (*33*). This matches the pK_a of the proton donor, zinc-bound water, suggesting that the pK_a of the donor and acceptor groups must be matched to optimize proton transfer.

Finally, a solvent-exposed and conformationally mobile proton shuttle group appears to be required. Conformational mobility of CA proton shuttles has been observed consistently (*32*, *34*, *35*). This flexibility may facilitate proton transfer from the active site cleft to buffer. Facile access to bulk solvent is clearly crucial for the efficient elimination of a proton from the active site of an enzyme.

ACKNOWLEDGMENT

This research was carried out in part at the National Synchrotron Light Source (NSLS), Brookhaven National Laboratory, which is supported by the U.S. Department of Energy, Division of Materials Sciences and Division of Chemical Sciences. We also thank Dr. Dieter Schneider and the staff of beamline X12C at the NSLS for support and assistance during data collection.

REFERENCES

1. Silverman, D. N., and Lindskog, S. (1988) *Acc. Chem. Res. 21*, 30−36.
2. Lindskog, S., and Liljas, A. (1993) *Curr. Opin. Struct. Biol. 3*, 915−920.
3. Christianson, D. W., and Fierke, C. A. (1996) *Acc. Chem. Res. 29*, 331−339.
4. Mori, K., Ogawa, Y., Ebihara, K., Tamura, N., Tashiro, K., Kuwahara, T., Mukoyama, M., Sugawara, A., Ozaki, S., Tanaka, I., and Nakao, K. (1999) *J. Biol. Chem. 274*, 15701−15705.
5. Khalifah, R. G. (1971) *J. Biol. Chem. 246*, 2561−2573.
6. Dodgson, S. J. (1991) in *The Carbonic Anhydrases* (Dodgson, S. J., Tashian, R. E., Gros, G., and Carter, N. D., Eds.) pp 297−306, Plenum Press, New York.
7. Heck, R. W., Tanhauser, S. M., Manda, R., Tu, C., Laipis, P. J., and Silverman, D. N. (1994) *J. Biol. Chem. 269*, 24742−24746.
8. Liljas, A., Kannan, K. K., Bergstén, P.-C., Waara, I., Fridborg, K., Strandberg, B., Carlbom, U., Järup, L., Lövgren, S., and Petef, M. (1972) *Nat. New Biol. 235*, 131−137.
9. Håkansson, K., Carlsson, M., Svensson, L. A., and Liljas, A. (1992) *J. Mol. Biol. 227*, 1192−1204.
10. Boriack-Sjodin, P. A., Heck, R. W., Laipis, P. J., Silverman, D. N., and Christianson, D. W. (1995) *Proc. Natl. Acad. Sci. U.S.A. 92*, 10949−10953.
11. Tu, C., Silverman, D. N., Forsman, C., Jonsson, B.-H., and Lindskog, S. (1989) *Biochemistry 28*, 7913−7918.
12. Steiner, H., Jonsson, B.-H., and Lindskog, S. (1975) *Eur. J. Biochem. 59*, 253−259.
13. Heck, R. W., Boriack-Sjodin, P. A., Qian, M., Tu, C., Christianson, D. W., Laipis, P. J., and Silverman, D. N. (1996) *Biochemistry 35*, 11605−11611.
14. Grotthuss, C. J. T. (1806) *Ann. Chim. 58*, 54−74.
15. Agmon, N. (1995) *Chem. Phys. Lett. 244*, 456−462.
16. Earnhardt, J. N., Qian, M., Tu, C., Laipis, P. J., and Silverman, D. N. (1998) *Biochemistry 37*, 7649−7655.
17. Earnhardt, J. N., Wright, S. K., Qian, M., Tu, C., Laipis, P. J., Viola, R. E., and Silverman, D. N. (1999) *Arch. Biochem. Biophys. 361*, 264−270.
18. Otwinowski, Z., and Minor, W. (1997) *Methods Enzymol. 276*, 307−326.
19. Collaborative Computational Project, Number 4 (1994) *Acta Crystallogr. D50*, 760−763.
20. Navaza, J. (1994) *Acta Crystallogr. A50*, 157−163.

21. Berman, H. M., Westbrook, J., Feng, Z., Gilliland, G., Bhat, T. N., Weissig, H., Shindyalov, I. N., and Bourne, P. E. (2000) *Nucleic Acids Res. 28*, 235−242.
22. Jones, T. A., Zou, J. Y., Cowan, S. W., and Kjeldgaard, M. (1991) *Acta Crystallogr. A47*, 110−119.
23. Brünger, A. T., Adams, P. D., Clore, G. M., DeLano, W. L., Gros, P., Grosse-Kunstleve, R. W., Jiang, J. S., Kuszewski, J., Nilges, M., Pannu, N. S., Read, R. J., Rice, L. M., Simonson, T., and Warren, G. L. (1998) *Acta Crystallogr. D54*, 905−921.
24. Whittington, D. A., Waheed, A., Ulmasov, B., Shah, G. N., Grubb, J. H., Sly, W. S., and Christianson, D. W. (2001) *Proc. Natl. Acad. Sci. U.S.A. 98*, 9545−9550.
25. Mohamadi, F., Richards, N. G. J., Guida, W. C., Liskamp, R., Lipton, M., Caufield, C., Chang, G., Hendrickson, T., and Still, W. C. (1990) *J. Comput. Chem. 11*, 440−467.
26. Kleywegt, G. J. (1995) *ESF/CCP4 Newsletter 31*, 45−50.
27. Kleywegt, G. J. (1996) *ESF/CCP4 Newsletter 32*, 32−36.
28. Kleywegt, G. J., and Jones, T. A. (1997) *Methods Enzymol. 277*, 208−230.
29. Wright, S. K., and Viola, R. E. (1998) *Anal. Biochem. 265*, 8−14.
30. Håkansson, K., Briand, C., Zaitsev, V., Xue, Y., and Liljas, A. (1994) *Acta Crystallogr. D50*, 101−104.
31. Pomès, R. (1999) *Isr. J. Chem. 39*, 387−395.
32. Nair, S. K., and Christianson, D. W. (1991) *J. Am. Chem. Soc. 113*, 9455−9458.
33. Tripp, B. C., and Ferry, J. G. (2000) *Biochemistry 39*, 9232−9240.
34. Iverson, T. M., Alber, B. E., Kisker, C., Ferry, J. G., and Rees, D. C. (2000) *Biochemistry 39*, 9222−9231.
35. Krebs, J. F., Fierke, C. A., Alexander, R. S., and Christianson, D. W. (1991) *Biochemistry 30*, 9153−9160.

BI015808Q